Coverage dependence and hydroperoxyl-mediated pathway of catalytic water formation on Pt (111) surface

Liang Qi, Jianguo Yu, and Ju Li[a)]
Department of Materials Science and Engineering, Ohio State University, Columbus, Ohio 43210

(Received 16 March 2006; accepted 21 June 2006; published online 1 August 2006)

Hydrogen oxidation on Pt (111) surface is modeled by density functional theory (DFT). Previous DFT calculations showed too large O_2 dissociation barriers, but we find them highly coverage dependent: when the coverage is low, dissociation barriers close to experimental values (~0.3 eV) are obtained. For the whole reaction, a new pathway involving hydroperoxyl (OOH) intermediate is found, with the highest reaction barrier of only ~0.4 eV. This may explain the experimental observation of catalytic water formation on Pt (111) surface above the H_2O desorption temperature of 170 K, despite that the direct reaction between chemisorbed O and H atoms is a highly activated process with barrier ~1 eV as previous calculations showed. © *2006 American Institute of Physics*. [DOI: 10.1063/1.2227388]

I. INTRODUCTION

The oxidation of hydrogen on platinum surface is a famous example of catalytic reaction. On contact with Pt (111) surface, gaseous H_2 and O_2 react at room temperature or below to produce water. Being a well-defined and characterized "model" system, this reaction is of fundamental importance to catalysis and electrocatalysis. Many theoretical calculations have been performed in the framework of density functional theory (DFT), not only for the whole reaction,[1] but also its elementary steps such as O_2 adsorption and dissociation.[2–4] While these calculations have contributed a great deal to our understanding, a complete reconciliation with experiments is not yet achieved. In particular, the predicted O_2 dissociation rate appears to be too slow compared to experiments, as well as the rate of H_2O formation above the water molecule desorption temperature T_{des}, which is ~170 K on Pt(111) surface under ultrahigh vacuum (UHV) condition.

Völkening *et al.* observed hydrogen oxidation reaction in progress with scanning tunneling microscope (STM) and high-resolution electron energy loss spectroscopy (EELS).[5] Two distinct temperature regimes were seen. Below T_{des}, the adsorbed water has an autocatalytic effect and the oxidation occurs via disproportionation reactions. Above T_{des}, when water does not stay on the surface, it was postulated that water is formed by successive additions of adsorbed H (H^*) atoms to adsorbed O (O^*) atom:

$$H^* + O^* \rightarrow OH^*, \tag{1}$$

$$H^* + OH^* \rightarrow H_2O^*. \tag{2}$$

Michaelides and Hu studied this reaction pathway by DFT, starting from chemisorbed O^* and H^* atoms.[1] They found that reaction (1) is a highly activated process, with an activation barrier of 0.94 eV. The barrier of reaction (2) on the other hand is very small, only 0.21 eV.

However, this scenario does not seem to be congruent with the experimental observation[6] that Pt is still a potent catalyst above T_{des}. Taking $T=200$ K (Ref. 6) and trial frequency $\nu=10^{12}$/s, a barrier of 0.94 eV would correspond to O^* half-life of $\sim 10^4$ years. So either the DFT barrier for reaction (1) is off or there may be alternative reaction pathways. Recent DFT calculations for oxygen reduction reaction (ORR) under aqueous electrochemical conditions have indicated the possibility of O_2^* reacting directly with hydronium $H_3O^+(H_2O)_2$ to form OOH^* intermediates.[7–9] Experimentally, there is also some hint for this possibility.[10,11] It is therefore profitable for us to look at this hydroperoxyl-mediated pathway using DFT under nonaqueous condition.

H^* and O^* arise from the adsorption and dissociation of O_2 and H_2. The case of H_2 is simple and has been well studied:[12] basically H_2 can dissociate without barrier upon contact with Pt (111) surface. The situation with O_2 is more complex. A common conclusion of several UHV experiments[13–17] is that the dissociation of O_2 on Pt (111) is a thermally activated process via molecular precursor states (MPSs), such as O_2^{-*} (superoxo, paramagnetic) or O_2^{2-*} (peroxo, nonmagnetic). Using DFT, Eichler and Hafner identified two energetically nearly degenerate precursors (O_2^{-*} at bridge site and O_2^{2-*} at fcc site), in excellent agreement with experiments. However, they also found that the O_2^* dissociation barriers were 0.8–0.9 eV,[2,3] which is definitely contradictory to the low experimental O_2 dissociation temperature estimated to be ~150 K.[13] Nolan *et al.* used EELS and molecular beam techniques to examine high translational energy adsorption of oxygen and estimated the dissociation barrier to be 0.29 eV.[17] Šljivančanin and Hammer recalculated the O_2^* dissociation barriers on flat Pt (111) surface and found the lowest barrier to be 0.6 eV,[18] which is good improvement. Recently Hyman and Medlin obtained the O_2 dissociation barrier to be 0.44 eV from a cluster calculation.[4] However,

a)Electronic mail: li.562@osu.edu

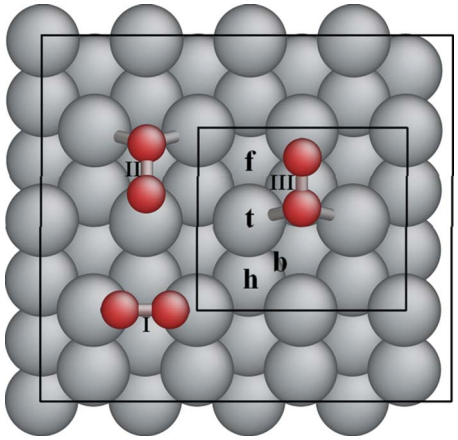

FIG. 1. Surface cell and short-hand notation of special sites, where there are three O_2^* adsorbed on bridge, fcc, and hcp hollow sites, respectively. The larger rectangle stands for $2\sqrt{3}\times4$ unit cell and the smaller one is for $\sqrt{3}\times2$.

the disagreement of slab calculation with experiments in O_2^* dissociation still exists and needs further study.

In this paper we use DFT to study the whole reaction process of water formation, starting from the adsorption of O_2 and H_2 on Pt (111). We resolve the two contradictions described above by searching for different reaction paths and checking the dependence of the energetics on adsorbate coverage. The latter could be fulfilled by changing the unit cell used in the calculation. In Sec. II, we give details of the calculation method. In Sec. III A, we discuss the problem of O_2 adsorption and dissociation. We verify the calculation by Michaelides and Hu for the (1)+(2) reaction in Sec. III B, then provide a new pathway starting from the direct protonation of O_2^* in Sec. III C. The results are summarized in Sec. IV.

II. COMPUTATIONAL METHOD

The calculations are performed using the Vienna *ab initio* simulation package (VASP) which is an efficient DFT code for extended systems.[19,20] We use the projector augmented wave (PAW) approach,[21,22] with Perdew-Burke-Ernzerhof (PBE) exchange-correlation functional.[23] The PAW potentials are generally more accurate than the ultrasoft (US) pseudopotentials[24,25] because the radial cutoffs (core radii) are smaller than the radii used for the US pseudopotentials and because PAW implicitly invokes the exact valence wave function with all nodes in the core region during the variational minimization. In all cases, the calculations are performed in spin-polarized condition with the plane wave expansion truncated at a cutoff kinetic energy of 400 eV.

The Pt (111) surface is modeled as a four-layer slab, separated by five layers equivalent of vacuum. In the most basic setup, we use a rectangular $\sqrt{3}\times2$ unit cell [leading to a $c(4\times2)$ structure] where there are four Pt atoms in each layer, and we use a Monkhorst-Pack k-point grid of $4\times4\times1$ for Brillouin-zone integration.[26] To check the effect of adsorbate coverage, we also increase the size of calculation supercell to $2\sqrt{3}\times4$ $[c(8\times4)]$ where there are 16 atoms in each layer, with a $2\times2\times1$ Monkhorst-Pack grid. All calculations are performed at the equilibrium Pt lattice constant of 3.977 Å as found from VASP geometry optimization (experimental lattice constant is 3.92 Å), while Pt atoms on the top two layers and the adsorbate atoms are allowed to relax freely. Figure 1 shows the surface unit cell and some special sites on it (t-top, b-bridge, f-fcc hollow, and h-hcp hollow).

TABLE I. O_2^* geometry in $\sqrt{3}\times2$ unit cell. The data in brackets are from Eichler and Hafner's results (Ref. 2). Here O_2-surface distance is the perpendicular distance between O_2 molecule center and surface plane. O_2 tilt angle is formed by O_2 molecular axis and surface plane, so 0° means O_2 is parallel to surface. All lengths are in angstroms and angles in degrees.

	O_2 bond length	O_2-surface distance	O_2 tilt angle
Bridge	1.35(1.39)	1.91(1.92)	0.0(0.0)
fcc	1.39(1.43)	1.76(1.78)	8.9(10.1)
hcp	1.38(1.42)	1.82(1.81)	8.1(8.4)

Reaction pathways are searched with the climbing image nudged elastic band (CI-NEB) method.[27] The nudged elastic band (NEB) is a method for finding saddle points and minimum energy paths between known reactants and products.[28,29] The method works by optimizing a number of intermediate images along the reaction path. Each image finds the lowest energy possible while maintaining equal spacing to neighboring images. This is done by adding spring forces along the band between images and by projecting out the force component parallel to the band due to the interatomic potential. The CI-NEB is a small modification of the NEB method in which the highest-energy image is driven up to the saddle point, trying to maximize its energy along the band and minimize in all other directions. When the algorithm converges, the highest-energy image will be at an exact saddle point, so less number of intermediate images is needed in CI-NEB than NEB. In this work, four intermediate images are used in searching for the saddle point of each elementary reaction step mentioned below, and the spring constant between adjacent images is 5.0 eV/Å^2.

III. RESULTS

A. H_2 and O_2 adsorption and dissociation

In $\sqrt{3}\times2$ unit cell, when H_2 molecule is close to the Pt surface, it would immediately dissociate into two H atoms adsorbed to the surface during relaxation, which means that there are no or very low dissociation barriers. It is found that H atoms preferentially occupy hollow sites. Nevertheless, the

TABLE II. O_2 adsorption energy on different sites and unit cells. The data in brackets are from Eichler and Hafner's results (Ref. 2). Here 2fcc (2hcp) means O_2 already dissociates into two O atoms in neighbor fcc (hcp) sites. All results are in eV.

	$\sqrt{3}\times2$ unit cell	$2\sqrt{3}\times4$ unit cell
Bridge	0.65(0.72)	0.67
fcc	0.53(0.68)	0.66
hcp	0.43(0.58)	0.46
2fcc	1.68	2.21
2hcp	1.21	1.49

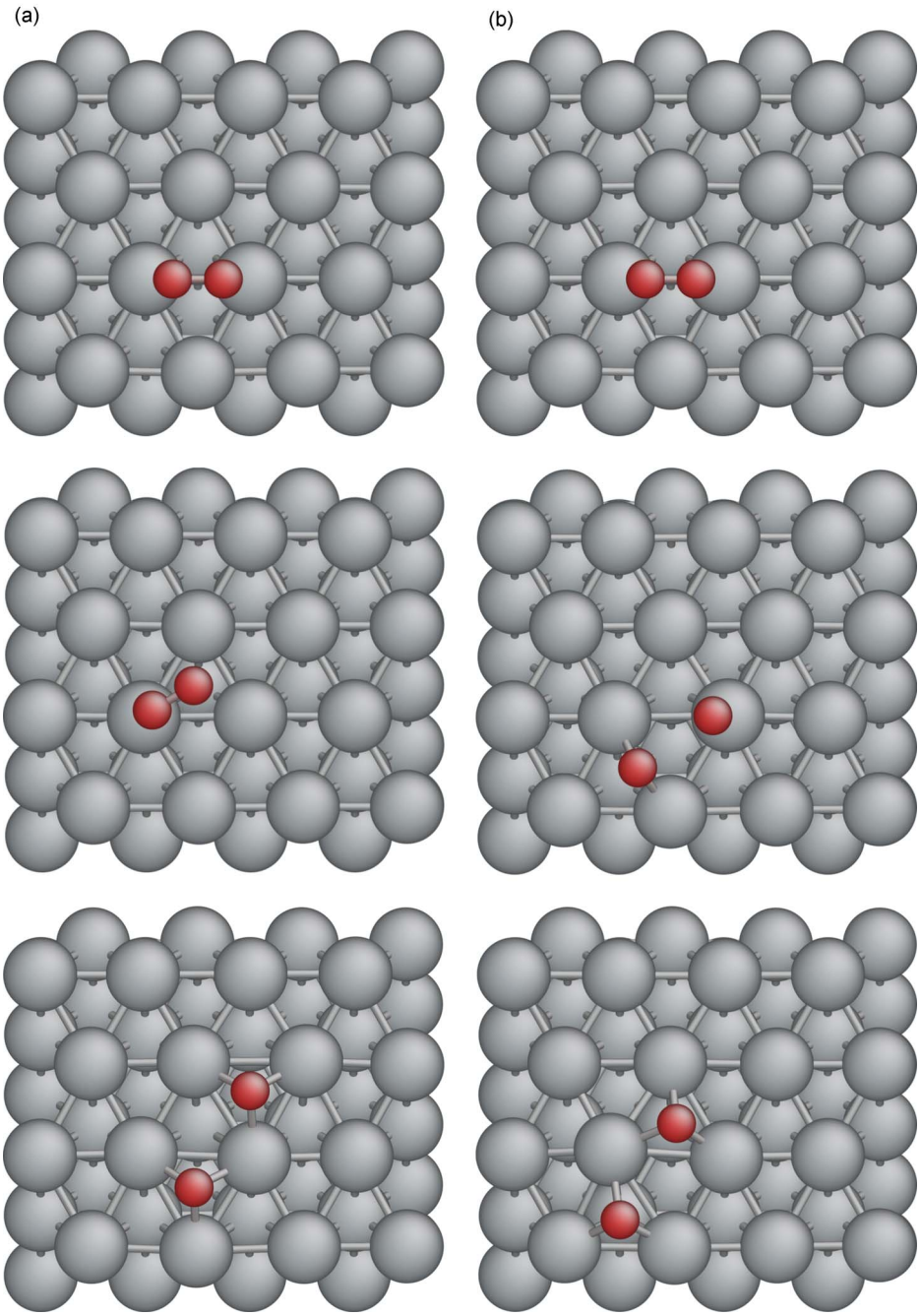

FIG. 2. The initial, transition, and final states for the reaction path of O_2 dissociation ($O_2^* \rightarrow 2O^*$) in $2\sqrt{3}\times 4$ unit cell. Although initial states are both O_2^* at bridge site, (a) shows the path to the final state with two O atoms at fcc sites and (b) shows the path to the final state with two O atoms at hcp sites.

difference in adsorption energy between various sites is very small, less than 0.02 eV. All these results agree well with previous DFT calculations.[12,30]

For oxygen in $\sqrt{3}\times 2$ unit cell, we first obtain the three chemisorbed O_2^* precursors,[2] shown in Fig. 1. Precursor I sits on the bridge site with molecular axis parallel to the surface and each oxygen atom binding to one Pt atom near the top site. Precursor II (III) sits on fcc (hcp) hollow site with one oxygen atom binding to Pt atom near top site and another binding to two Pt atoms at the bridge site, respectively. The geometrical parameters are listed in Table I. The adsorption energies at these three sites are similar to the results of Eichler and Hafner,[2] as shown in Table II. The differences in geometries and adsorption energy may come from the usage of different pseudopotentials (Eichler and Hafner used ultrasoft pseudopotentials). By inspecting the local density of states (LDOS) on oxygen atoms, we determine that the most stable $(O_2^*)_{\text{bridge}}$ species is O_2^-, while $(O_2^*)_{\text{fcc}}$ and $(O_2^*)_{\text{hcp}}$ are O_2^{2-}. The stability ranking of charged adsorbates is of course a function of the electrical double layer (EDL) that spans the adsorbate and the surface, or equivalently the surface work function which is coverage dependent.[31] Present results may switch order at some other Pt potentials.

We then increase the unit cell to $2\sqrt{3}\times 4$ and find the adsorption energy increases by ~0.1 eV for O_2 at fcc site but is almost unchanged for the other two sites. The dissociation energy of O_2^* is calculated by placing two O atoms in two neighboring fcc or hcp hollow sites. Surprisingly, Table II shows that it increases a lot from the small unit cell to the large unit cell, especially for O atom at fcc hollow site,

TABLE III. Geometries of O_2^* dissociation paths in $2\sqrt{3}\times4$ unit cell. As Fig. 2 shows, $O_a(O_b)$ is the left(right) oxygen atom in the initial state. Here d_{O-O} is the distance between two oxygen atoms. d_{Pt-O} is the distance between O atom and its nearest Pt atom. d_z is the perpendicular distance between O atom and Pt surface. I, $T1(T2)$, and $F1(F2)$ stand for the initial, transition, and final states for path 1(2). All lengths are in angstroms.

	d_{O-O}	d_{Pt-O_a}	$d_z(O_a)$	d_{Pt-O_a}	$d_z(O_b)$
I	1.35	2.04	1.90	2.04	1.90
$T1$	1.32	2.01	1.99	2.75	2.25
$F1$	3.01	2.03	1.14	2.04	1.14
$T2$	2.51	1.98	1.31	1.83	1.78
$F2$	3.02	2.03	1.24	2.03	1.25

which is much more attractive for O than hcp hollow site.[32] This indicates the strong dependence of O atom adsorption energy on O coverage. It should also affect the dissociation barriers according to Bronsted-Evans-Polanyi relation.[33]

The next step is to calculate the O_2 dissociation barrier. From the above we think that when the unit cell is small there may be strong lateral interactions between O^*'s, which may be mediated via the competition for metal's electron. To minimize this effect on O_2 dissociation, we first use $2\sqrt{3}\times4$ unit cell to calculate the dissociation barrier. O_2^* at bridge site is used as the initial state, and the final state will be two O^* in two hollow sites. Although O^* is much more stable at fcc hollow site than at hcp hollow site, two O^* at two hcp hollow sites could also be the final state of oxygen dissociation since it is also a local minimum and can be an intermediate state along the whole reaction path. For this reason, two different reaction paths are chosen, which are from bridge site to two fcc hollow sites and from bridge site to two hcp hollow sites, respectively, as shown in Fig. 2. In the first path, O_2 molecule rotates towards the fcc hollow site with one oxygen atom still bonding with Pt near the top site and stays molecular at the transition state. In the second path, oxygen molecule rotates towards the hcp hollow site in a similar way. However, at the transition state oxygen-oxygen bond is already broken. The geometries are given in Table III. The barrier energies are 0.37 and 0.27 eV for path 1 and path 2, respectively. These low dissociation barriers agree well with several experimental results.[13,17]

However, if the unit cell decreases to $\sqrt{3}\times2$, although the geometries of the saddle points do not change very much, the dissociation barriers increase a lot. The barrier of path 2 mentioned above increases to 0.52 eV, which again illustrates the strong dependence on oxygen coverage. This could also explain the overestimation of the dissociation barrier by previous DFT calculations. In Eichler and Hafner's calculation, the unit cell was $\sqrt{3}\times2$ and the activation energy was explored only on fixed paths.[2] In Šljivančanin and Hammer's calculation,[18] a larger unit cell was used, but it was still smaller than $2\sqrt{3}\times4$. Generally a trend can be identified here that when O_2 coverage is small, it is much easier to dissociate.

B. Water formation from chemisorbed O^* and H^* atoms

After obtaining the chemisorbed O^* and H^* atoms, the work that remains is just to add H^* to O^* one by one. The calculations have been performed by Michaelides and Hu, and they are repeated here just for consistency check. The energetic results from both sources are almost identical, as shown in Table IV.

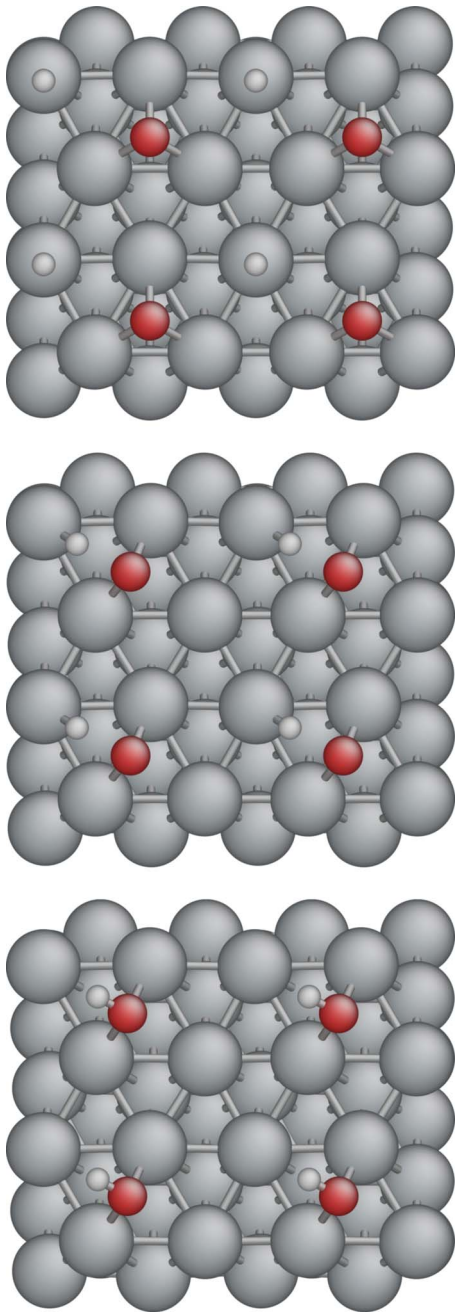

FIG. 3. The initial, transition, and final states for the reaction path of OH formation ($O^*+H^*\rightarrow OH^*$) in $\sqrt{3}\times2$ unit cell.

The detailed reaction path in $\sqrt{3}\times2$ unit cell is shown in Figs. 3 and 4 and some important geometrical parameters are

TABLE IV. The reaction energy (ΔE) and activation barrier (E_a) of reaction path of water formation from O^* and H^* atoms. Data in brackets are from Michaelides and Hu (Ref. 1)

	ΔE [eV]	E_a [eV]
$O^*+H^*\rightarrow OH^*$	−0.20	0.91(0.94)
$OH^*+H^*\rightarrow H_2O^*$	−0.75	0.14(0.21)

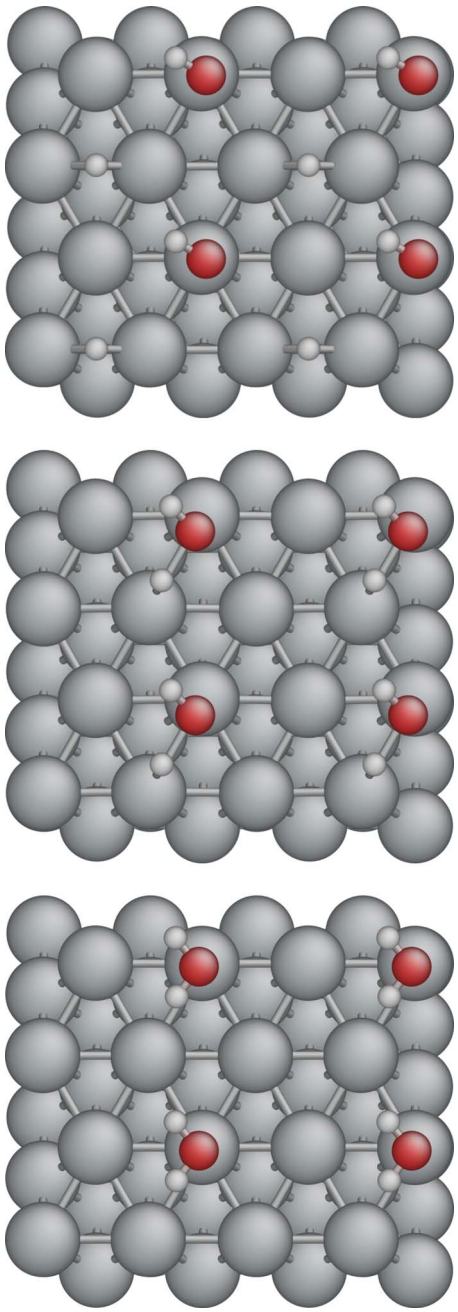

FIG. 4. The initial, transition, and final states for the reaction path of H_2O formation ($OH^*+H^* \rightarrow H_2O^*$) in $\sqrt{3}\times 2$ unit cell.

given in Tables V and VI, respectively. For reaction (1), the initial state is O at the fcc hollow site and H at the top site (Fig. 3), then O and H atoms come close to each other along ⟨112⟩ direction and finally OH stays at bridge site with O atom connected to two nearby Pt atoms. Meanwhile, it is

TABLE V. Geometries of initial (I), transition (T), and final (F) states of reaction (1) in $\sqrt{3}\times 2$ unit cell. The notation follows Table III. All lengths are in angstroms.

	d_{O-H}	d_{Pt-O}	$d_z(O)$	d_{Pt-H}	$d_z(H)$
I	3.22	2.05	1.16	1.56	1.56
T	1.59	2.05	1.44	1.67	1.30
F	0.99	2.17	1.63	2.59	2.01

TABLE VI. Geometries of initial (I), transition (T), and final (F) states of reaction (2) in $\sqrt{3}\times 2$ unit cell. There are two H atoms and H_a is the one which is initially absorbed separately on Pt surface. The notation follows Table III. All lengths are in angstroms.

	d_{O-H_a}	d_{Pt-O}	$d_z(O)$	d_{Pt-H_a}	$d_z(H_a)$
I	3.89	2.00	1.99	1.75	1.05
T	1.68	2.06	2.01	1.64	1.43
F	0.98	2.48	2.48	2.72	2.49

calculated that OH at the top site is only 0.02 eV less stable than OH at bridge site so we can consider them as nearly degenerate intermediate states. As Michaelides and Hu mentioned, a lot of the energy barrier comes from O^* diffusion, since at the saddle point O^* moves from the fcc hollow site to a bridgelike site. We have previously calculated isolated O^* atom diffusion barrier from the fcc site to the neighboring hcp site to be 0.62 eV, which is a significant fraction of the reaction (1) barrier. After OH formation, adding another H to it is very easy. As shown in Fig. 4, during reaction (2) O atom always stays close to the top site and only H^* atom needs to make large movements, which costs small amount of energy as calculated in Sec. III A. We also check the coverage effect on the barrier of OH formation and find that it just increases a little, from 0.91 to 1.0 eV, when the unit cell changes to $2\sqrt{3}\times 4$. This means the coverage dependence of reaction (1) is smaller than that of oxygen dissociation.

C. Water formation from chemisorbed O_2^* molecule and H^* atoms

In Sec. III B, the barrier of OH formation seems too high for Pt to be a reasonably good catalyst above $T_{des} \sim 170$ K. There may be some explanations for this; for example, there could be other sites such as steps, kinks, and other defects.[34] However, here we offer a possible intrinsic mechanism. It involves the direct protonation of O_2^* molecular precursors (Table VII),

$$O_2^* + H^* \rightarrow OOH^*, \tag{3}$$

followed by

$$OOH^* + H^* \rightarrow 2OH^*, \tag{4}$$

and then reaction (2), because O_2^* has a finite lifetime on the platinum surface. Indeed, as shown in Sec. III A, the O_2^* dissociation barrier is strongly dependent on the coverage, so O_2^* may exist for much longer time on Pt (111) surface if P_{O_2} is large. The Langmuir-Hinshelwood pathway we propose here differs from the Eley-Rideal pathways studied theoretically before,[7–9] in that H^* is already adsorbed on the surface

TABLE VII. The reaction energy (ΔE) and activation barrier (E_a) of reaction path of water formation from O_2^* molecule and H^* atom.

	ΔE (eV)	E_a (eV)
$O_2^*+H^* \rightarrow OOH^*$	−0.18	0.42
$OOH^*+H^* \rightarrow 2OH^*$	−2.19	0.31
$OH^*+H^* \rightarrow H_2O^*$	−0.75	0.14

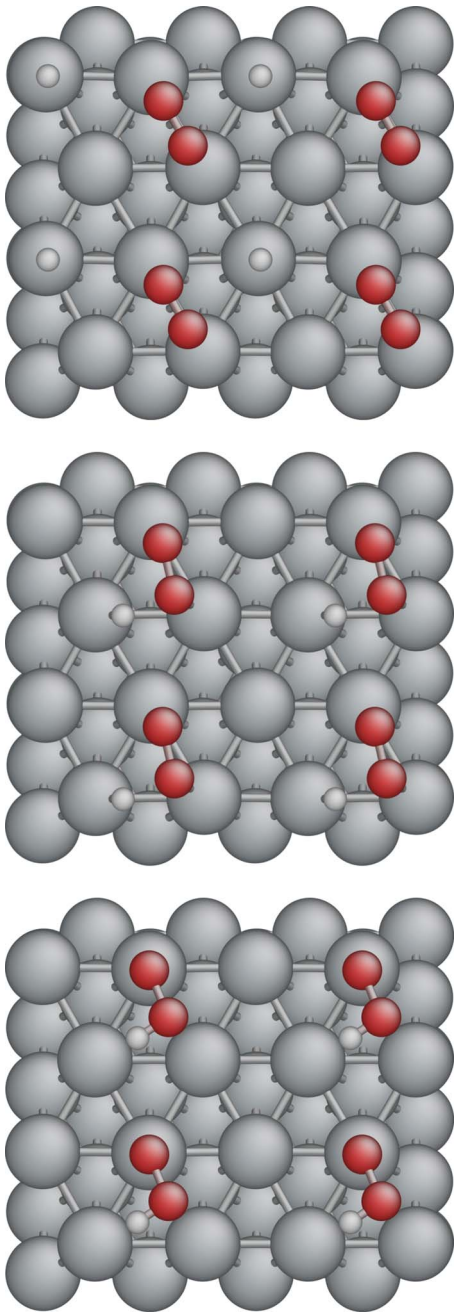

FIG. 5. The initial, transition, and final states for the reaction path of OOH formation ($O_2^*+H^* \rightarrow OOH^*$) in $\sqrt{3}\times 2$ unit cell.

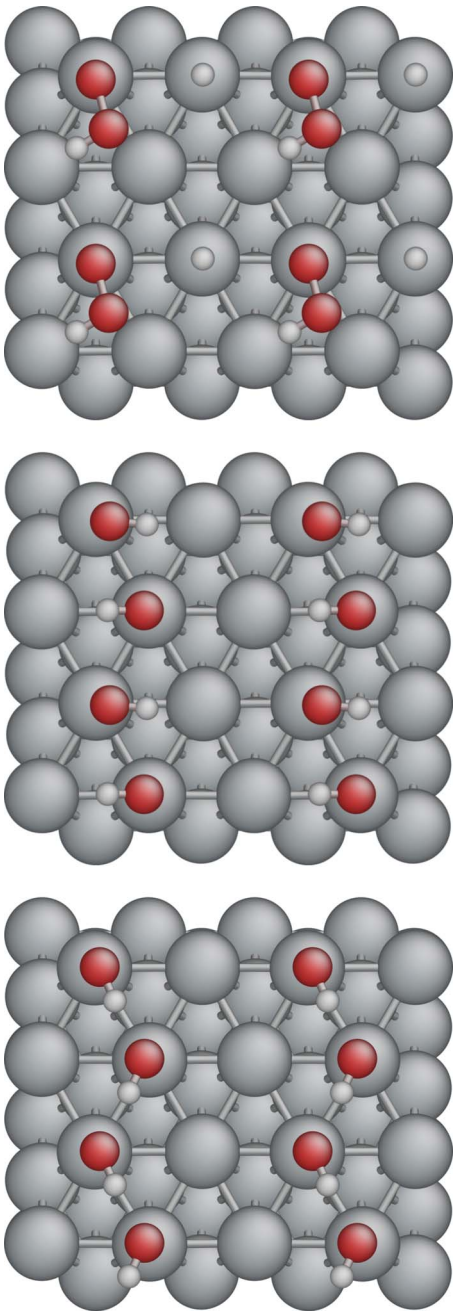

FIG. 6. The initial, transition, and final states for the reaction path of 2OH formation ($OOH^*+H^* \rightarrow 2OH^*$) in $\sqrt{3}\times 2$ unit cell.

and stays close to the surface during the reaction.

The path we obtain is the following. As shown in Fig. 5, initially O_2^* is at bridge site and H^* at a top site nearby. Then H^* comes close to O_2^* and directly forms a hydroperoxyl intermediate OOH^*, which has one O atom connected to Pt at top site and the remaining OH part a little away from the surface. However, the two O atoms still connect to each other and stay around the bridge site. The geometry is given in Table VIII. Although there are large movements of the two O atoms, they always stay bonded during the whole process, and it costs only 0.42 eV energy to reach the saddle point.

TABLE VIII. Geometries of initial (I), transition (T), and final (F) states of reaction (3) in $\sqrt{3}\times 2$ unit cell. There are two O atoms: O_a is the one which is finally connected with H atom and O_b is the other one. The notation follows Table III. All lengths are in angstroms.

	d_{O_a-H}	$d_{O_a-O_b}$	d_{Pt-O_a}	$d_z(O_a)$	d_{Pt-O_b}	$d_z(O_b)$	d_{Pt-H}	$d_z(H)$
I	4.80	1.35	2.06	1.94	2.06	1.94	1.56	1.56
T	1.56	1.41	2.14	1.93	2.03	1.93	1.64	1.47
F	0.99	1.43	2.88	2.52	2.01	2.01	3.02	2.59

In the next step, there are two possible choices: one is that OOH^* dissociates to one O^* and one OH^*, but then it comes back to the previous reaction pathway where there is still a large barrier to form OH^* from isolated O^*; the other is directly adding another H atom to this OOH^* to form two isolated OH^*. The minimum energy path is shown in Fig. 6 and some geometrical parameters are given in Table IX. Ini-

TABLE IX. Geometries of initial (I), transition (T), and final (F) states of reaction (4) in $\sqrt{3}\times 2$ unit cell. There are two O atoms: O_a is the one which is initially connected with H atom and O_b is the other one. Similarly, H_a is the H atom initially connected with O atom and H_b is the other. The notation follows Table III. All lengths are in angstroms.

	$d_{O_b-H_b}$	$d_{O_a-O_b}$	d_{Pt-O_a}	$d_z(O_a)$	d_{Pt-O_b}	$d_z(O_b)$	d_{Pt-H_b}	$d_z(H_b)$
I	2.87	1.43	2.87	2.48	2.02	2.02	1.56	1.56
T	1.50	1.48	2.47	2.33	2.16	2.04	1.67	1.42
F	1.01	2.70	2.00	1.99	1.99	1.99	2.44	2.22

tially both OOH^* and H^* are at top sites. Finally there are two OH^* at two neighboring top sites, forming a chain of hydrogen bonds. The barrier energy is only 0.31 eV. The whole reaction can then finish via (2).

The reason for the low barrier of (3) is that there is no motion of isolated O^* atom on the surface, which has been shown to involve a large energy barrier. Since the reaction starts from a whole O_2^* molecule, this path could be important when the oxygen coverage is high so that the O_2^* dissociation barrier is large enough to keep O_2^* existing for a while. This is possible, since in $\sqrt{3}\times 2$ unit cell O_2^* dissociation barrier is higher than the OOH^* formation barrier. Another problem with this new path is that OOH^* may not be a long-lived intermediate,[11] because it could dissociate into O^* and OH^* quickly. However, if there are a lot of H^* atoms around (large P_{H_2}), this path is still possible.

The whole reactions (1)+(2) and (3)+(4)+(2) are compared in Fig. 7. Obviously, no matter which catalyst and which path are chosen, the total reaction energy should be a constant, which is −5.08 eV from isolated molecule DFT calculations with the parameter setting described in Sec. II. However, this number cannot be obtained by simply adding the individual step reaction energies, due to lateral interactions in the small calculation cell. For example, in $\sqrt{3}\times 2$ unit cell, if we compare the energy of surface plus one adsorbed O^* atom, surface plus one absorbed H^* atom, and surface plus both adsorbed O^* and H^* atoms, it is found that there is a repulsion energy of 0.12 eV between O^* and H^*. So the real reaction energy of (1) should be added by 0.12 eV in $\sqrt{3}\times 2$ unit cell. By adding this kind of corrections to the initial and final states of all elementary reaction steps, the whole reaction paths are drawn in Fig. 7, where the net reaction energy is −5.08 eV in both cases.

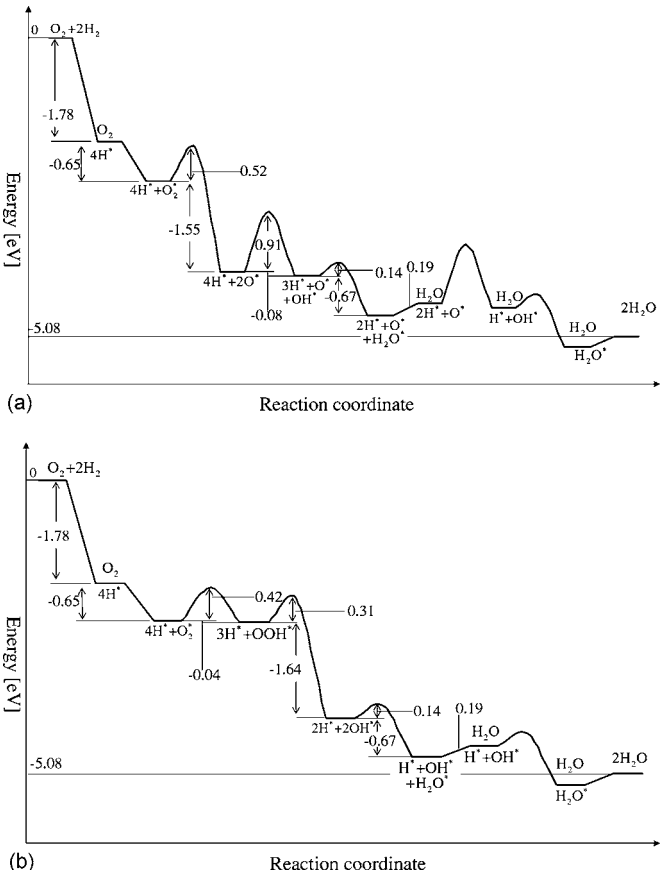

FIG. 7. The whole reaction path of water formation: (a) shows the path starting by dissociation of O_2^* and (b) shows the path starting by formation of OOH^*.

IV. CONCLUSION

In this paper we offer possible resolutions of two contradictions that have existed between experiments and DFT calculations concerning hydrogen oxidation on Pt (111) surface. First, although oxygen molecules are known to dissociate at ~150 K under UHV condition experimentally, previous calculations gave quite large O_2^* dissociation barriers. In our study we find that this may result from the usage of small unit cell in calculation. If the unit cell is large enough ($2\sqrt{3}\times 4$ in our case), the O_2^* dissociation barrier becomes reasonable (~0.3 eV). This also indicates strong dependence of the O_2^* dissociation barrier on oxygen coverage. Second, previous DFT study on the OH formation showed that there is a reaction barrier as high as ~1 eV. In our study, we verified that this value is correct for the reaction path proposed, and that it is not very coverage sensitive. But we propose a new reaction path of directly protonating O_2^* via the Langmuir-Hinshelwood mechanism to form OOH^* (hydroperoxyl), which only involves an energy barrier of ~0.4 eV. This path may be important when P_{O_2} and P_{H_2} are both high.

ACKNOWLEDGMENTS

We acknowledge support by Honda Research Institute USA, Inc. and the Ohio Supercomputer Center and thank Joshua Fujiwara for helpful discussions.

[1] A. Michaelides and P. Hu, J. Am. Chem. Soc. **123**, 4235 (2001).
[2] A. Eichler and J. Hafner, Phys. Rev. Lett. **79**, 4481 (1997).
[3] A. Eichler, F. Mittendorfer, and J. Hafner, Phys. Rev. B **62**, 4744 (2000).
[4] M. P. Hyman and J. W. Medlin, J. Phys. Chem. B **109**, 6304 (2005).

[5] S. Völkening, K. Bedürftig, K. Jacobi, J. Wintterlin, and G. Ertl, Phys. Rev. Lett. **83**, 2672 (1999).
[6] P. R. Norton, J. Catal. **36**, 211 (1975).
[7] R. A. Sidik and A. B. Anderson, J. Electroanal. Chem. **528**, 69 (2002).
[8] Y. X. Wang and P. B. Balbuena, J. Phys. Chem. B **108**, 4376 (2004).
[9] Y. X. Wang and P. B. Balbuena, J. Phys. Chem. B **109**, 14896 (2005).
[10] L. K. Verheij and M. B. Hugenschmidt, Surf. Sci. **416**, 37 (1998).
[11] J. Biener, E. Lang, C. Lutterloh, and J. Küppers, J. Chem. Phys. **116**, 3063 (2002).
[12] R. A. Olsen, G. J. Kroes, and E. J. Baerends, J. Chem. Phys. **111**, 11155 (1999).
[13] J. L. Gland, B. A. Sexton, and G. B. Fisher, Surf. Sci. **95**, 587 (1980).
[14] H. Steininger, S. Lehwald, and H. Ibach, Surf. Sci. **123**, 1 (1982).
[15] D. A. Outka, J. Stohr, W. Jark, P. Stevens, J. Solomon, and R. J. Madix, Phys. Rev. B **35**, 4119 (1987).
[16] B. C. Stipe, M. A. Rezaei, W. Ho, S. Gao, M. Persson, and B. I. Lundqvist, Phys. Rev. Lett. **78**, 4410 (1997).
[17] P. D. Nolan, B. R. Lutz, P. L. Tanaka, J. E. Davis, and C. B. Mullins, J. Chem. Phys. **111**, 3696 (1999).
[18] Z. Šljivančanin and B. Hammer, Surf. Sci. **515**, 235 (2002).
[19] G. Kresse and J. Furthmüller, Comput. Mater. Sci. **6**, 15 (1996).
[20] G. Kresse and J. Furthmüller, Phys. Rev. B **54**, 11169 (1996).
[21] P. E. Blöchl, Phys. Rev. B **50**, 17953 (1994).
[22] G. Kresse and D. Joubert, Phys. Rev. B **59**, 1758 (1999).
[23] J. P. Perdew, K. Burke, and M. Ernzerhof, Phys. Rev. Lett. **77**, 3865 (1996).
[24] D. Vanderbilt, Phys. Rev. B **41**, 7892 (1990).
[25] S. Ogata, J. Li, and S. Yip, Science **298**, 807 (2002).
[26] H. J. Monkhorst and J. D. Pack, Phys. Rev. B **13**, 5188 (1976).
[27] G. Henkelman, B. P. Uberuaga, and H. Jonsson, J. Chem. Phys. **113**, 9901 (2000).
[28] G. Henkelman and H. Jonsson, J. Chem. Phys. **113**, 9978 (2000).
[29] T. Zhu, J. Li, and S. Yip, Phys. Rev. Lett. **93**, 025503 (2004).
[30] G. W. Watson, R. P. K. Wells, D. J. Willock, and G. J. Hutchings, J. Phys. Chem. B **105**, 4889 (2001).
[31] G. N. Derry and P. N. Ross, J. Chem. Phys. **82**, 2772 (1985).
[32] P. J. Feibelman, Phys. Rev. B **56**, 10532 (1997).
[33] T. Bligaard, J. K. Norskov, S. Dahl, J. Matthiesen, C. H. Christensen, and J. Sehested, J. Catal. **224**, 206 (2004).
[34] L. K. Verheij, M. Freitag, M. B. Hugenschmidt, I. Kempf, B. Poelsema, and G. Comsa, Surf. Sci. **272**, 276 (1992).